Received: 7 May 2022 | Revised: 8 August 2022 | Accepted: 4 September 2022

DOI: 10.1111/jace.18782

Journal of the American Ceramic Society

RESEARCH ARTICLE

Working mechanism of calcium nitrate as an accelerator for Portland cement hydration

Tobias Dorn | **Tamino Hirsch** | **Dietmar Stephan**

Institute of Civil Engineering, Group of Building Materials and Construction Chemistry, Technische Universität Berlin, Berlin, Germany

Correspondence
Dietmar Stephan, Institute of Civil Engineering, Group of Building Materials and Construction Chemistry, Technische Universität Berlin, 13355 Berlin, Germany.
Email: stephan@tu-berlin.de

Funding information
German Federal Ministry of Education and Research, Grant/Award Number: 03XP0122A

Abstract

Precast concrete, cold weather concreting, and the emerging technique of concrete additive manufacturing are applications in which the acceleration of cement hydration plays a critical role. To allow precise control of early cement hydration in these applications, a thorough understanding of the working mechanisms of cement hydration accelerators is required. This study contributes to the understanding of the mechanism by which calcium nitrate ($Ca(NO_3)_2$) influences early cement hydration. The influence of $Ca(NO_3)_2$ on the hydration of an ordinary Portland cement has been followed by isothermal calorimetry, in situ X-ray diffraction (XRD), quantitative XRD, compressive strength testing, and the analysis of the pore solution composition. Further, the initial pore solution, the initial phase composition, and the phase composition in the fully hydrated cement have been estimated by thermodynamic calculations to corroborate the experimentally obtained results. The results indicate that $Ca(NO_3)_2$, especially at the highest analyzed dosage of 5 wt.%, enhances the formation of ettringite and a nitrate-containing AFm phase. Furthermore, $Ca(NO_3)_2$ accelerates alite hydration. Besides the increased Ca concentration in solution, it has been found that a reduction of the Al concentration in the initial pore solution by $Ca(NO_3)_2$ possibly contributes to the accelerating effect of $Ca(NO_3)_2$ on alite hydration.

KEYWORDS
acceleration, additives, hydration, Portland cement, thermodynamics

1 | INTRODUCTION

The rate of ordinary Portland cement (OPC) hydration can be altered by adding several chemical substances, which, if they increase the rate of hydration, are referred to as accelerators. Accelerators can shorten the setting time (set accelerators), increase the rate of compressive strength development (hardening accelerators), or affect both, setting and hardening.[1] Important fields in which accelerators are used include the production of precast concrete and concreting at cold temperatures, which tend to significantly prolong setting times.[2–4] Recently, as extrusion-based additive manufacturing (AM) with mortar and concrete is gaining an increased interest in research and industrial application, a new field of accelerator application is emerging.[5] AM describes an automatically controlled process of layer-wise material deposition in which no formwork is used to support the freshly placed

material. Consequently, AM imposes high requirements on the dimensional stability of the material right after the deposition.[6] The addition of accelerators to the material within the printing nozzle shortly before the material deposition might be a good option for obtaining reliable AM processes. In such processes, a material with a sufficiently high flowability to continuously flow within the automatically operating 3D-printing system could be applied. Acceleration in the printing nozzle would spark a sufficiently fast strength gain after deposition for the material to support its own weight and the weight of subsequently deposited material layers.[7,8] However, to develop such AM processes, a precise knowledge of the working mechanisms of cement hydration accelerators is required.

Calcium nitrate is a frequently applied accelerator. $Ca(NO_3)_2$ was introduced as an accelerator for cement hydration during the 1980s[9] to replace chloride-containing accelerators such as calcium chloride ($CaCl_2$), the Cl^- ions of which had been shown to cause damage to the steel reinforcement by depassivation of the steel.[10,11] Since then, the effect of $Ca(NO_3)_2$ on the setting and hardening of OPC and the underlying mechanism were analyzed in several studies,[12–19] which have been summarized in a recently published review on cement hydration accelerators by Dorn et al.[20]

Regarding the influence of $Ca(NO_3)_2$ on the aluminate reaction, Balonis et al.,[14] based on thermodynamic calculations as well as experimental evaluations, suggested that the presence of NO_3^{2-} ions in solution results in the formation of nitrate-containing AFm phases (NO_3-AFm) at the expense of monosulfoaluminate (SO_4-AFm) or, in carbonate-containing systems, at the expense of monocarboaluminate (CO_3-AFm (mono)). NO_3-AFm formation was later confirmed to occur by Franke et al.[21] based on the analysis of ASTM I/II, and ASTM II/V-based cement pastes accelerated with $Ca(NO_3)_2$. In general, AFm phases are a group of cement hydration products forming platy hexagonal or pseudohexagonal crystals with the formula $[Ca_2Al(OH)_6](X)_y \cdot zH_2O$ in which X represents Cl^-, NO_3^-, $Al(OH)_4^-$, $(CO_3^{2-})_{0.5}$, or $(SO_4^{2-})_{0.5}$.[22–24]

Moreover, Hill et al.,[13] who analyzed the hydration of Class C fly ash in the presence of $Ca(NO_3)_2$, discussed the formation of nitrate-modified calcium aluminate hydrates. However, although Hill et al.[13] found that the formation of NO_3-AFm competes with the formation of ettringite (AFt) in Class C fly ash analyzed in their study, Balonis et al.,[14] as well as Abdelrazig et al.,[12] described an increased formation of ettringite in the presence of nitrate in solution for OPCs. According to Balonis et al.,[14] SO_4^{2-}, available in the SO_4-AFm phases, is replaced in the course of NO_3-AFm formation, and the consequently increased availability of SO_4^{2-} contributes to the increased ettringite formation.

Regarding the silicate reaction of OPC, it has been shown that $Ca(NO_3)_2$ shortens the time until the main hydration of alite starts, and it increases the rate of alite hydration and possibly also that of belite.[15–17,25] Justnes et al.[18] suggested that the dissolution of $Ca(NO_3)_2$ results in a fast supersaturation of the pore solution with respect to portlandite (CH), and that the resulting early precipitation of CH is responsible for the early onset and the increased rate of alit hydration. Nicoleau[26] argues that calcium salts allow the homogenous nucleation of C–S–H by increasing the availability of calcium in solution, and that this enhanced nucleation is responsible for the acceleration of alite hydration. In recent years, it has been regularly discussed that the onset of fast alite hydration in OPCs is retarded by aluminum in the pore solution.[27–33] Consequently, if $Ca(NO_3)_2$, by altering the C_3A hydration, reduces [Al] in the initial pore solution composition, this might be an aspect of alite hydration acceleration by $Ca(NO_3)_2$ that has not yet been fully considered.

The present study aims at evaluating the effect of $Ca(NO_3)_2$ in solution on the formation of AFm phases and ettringite in a hydrating commercial OPC more closely, as well as on analyzing the development of ion concentrations in the early pore solution composition in the dependence of $Ca(NO_3)_2$ addition.

Isothermal heat flow calorimetry was used to investigate the influence of $Ca(NO_3)_2$ on the reactivity of the analyzed OPC at any given time up to 72 h. In situ X-ray diffraction (in-situ XRD) was applied to experimentally analyze the dissolution of selected cement phases as well as the formation of crystalline hydration products during the first 24 h of hydration. At the same time, quantitative powder XRD (QXRD) was used to quantitatively determine the phase composition of the hydrated cement in the dependence of the $Ca(NO_3)_2$ addition at specific later times. The development of the pore solution composition of the OPC in dependence on $Ca(NO_3)_2$ addition during the first 60 min of hydration was analyzed by inductively coupled plasma optical emission spectroscopy (ICP-OES). The initial pore solution composition, the initial hydration product formation, and the phase composition of the fully hydrated cement were, furthermore, modeled by thermodynamic calculations in the dependence of the $Ca(NO_3)_2$ addition to corroborate the experimentally determined results.

2 | EXPERIMENTAL PROCEDURES

2.1 | Materials and methods

A commercial OPC (CEM I 52.5 R) and $Ca(NO_3)_2 \cdot 4H_2O$ produced by Alfa Aesar (Stock No. 12364, p.a.) have been

used in all experiments. The water contained in the calcium nitrate tetrahydrate was determined by drying to mass constancy at 110°C and was subtracted from the mixing water.

2.2 | Mixing proportions and mixing procedure

Samples are named according to the amount of $Ca(NO_3)_2$ that has been added to a specific sample. The number in the sample nomenclature indicates the added amount of $Ca(NO_3)_2$ in wt.% of cement. All experiments, except compressive strength testing on mortar prisms, have been performed using cement paste. Most samples have been prepared with a water to cement ratio (*w/c*) of 0.5. Samples prepared for the analysis of pore solution have been prepared with a *w/c* of 1. To obtain calorimetric results that correlate directly to all applied experimental techniques, isothermal heat flow calorimetry was performed on samples prepared with a *w/c* of 0.5 and 1.0.

Most samples were mixed for 2 min using a vortex mixer on the highest level. Samples prepared for compressive strength testing on cement paste cubes were mixed according to EN 196-3,[34] whereas mortar samples prepared for compressive strength testing on mortar prisms were mixed according to EN 196-1.[35] $Ca(NO_3)_2$ was added to the cement together with the mixing water in which it was dissolved at least 24 h before the initial contact of cement and water.

2.3 | Isothermal heat flow calorimetry

Isothermal heat flow calorimetry measurements were performed using a calorimeter (TAM Air, TA Instruments, USA) at 20°C. Samples were prepared with a *w/c* of 0.5 (3 g cement, 1.5 g water) and a *w/c* of 1.0 (1.72 g cement, 1.72 g water) to validate the results obtained from pore solution analysis. Mixing of the samples was performed outside the device. Each sample was placed in the device immediately after mixing. The heat flow of each sample was recorded over 72 h.

2.4 | X-ray diffraction (XRD)

All XRD experiments were performed using an XRD (Empyrean, PANalytical, the Netherlands) in Bragg–Brentano geometry, equipped with a Cu K_α radiation-emitting X-ray tube. For the in situ XRD measurements, ~5 g of cement paste were placed in a temperature-controlled sample stage set to 20°C. To protect the samples from evaporation and carbonation, the samples were covered with a *Kapton* film (thickness 7.5 μm) during the entire measurement. In situ XRD measurements were performed for a maximum duration of 24 h. Each measurement started 8 min after the initial contact of cement and water. During the measurement time, a scan in the range between 6° and 40° 2Θ was started every 10 min. For evaluating the in situ XRD results, reflex intensities were compared after background subtraction. Based on the comparison of reflex intensities, a qualitative conclusion has been drawn on the dissolution of cement phases and the formation of crystalline hydration products. The in situ XRD results have not been quantified as the quantification of in situ XRD results by Rietveld refinement faces several problems due to the continuous change of important parameters such as intensity of the measured background and crystalline phase content.

To obtain QXRD results, XRD measurements have been performed on hardened cement pastes. After 1, 7, and 28 days, the hydration was stopped by solvent exchange using ethanol. To obtain finely ground powders, which are crucial to obtain reproducible QXRD results, while avoiding amorphization of particles, the samples were wet ground after the intended hydration time in a special mill (McCrone, Retsch, Germany) using ethanol as grinding liquid. To quantify the amorphous content, 20 wt.% of rutile (TiO_2) was added as an internal standard to each sample before grinding. No internal standard was added to the anhydrous cement as amorphous content was expected to be too small for a precise determination.[36,37]

For the XRD measurements of the powdered samples, a fixed divergence slit (0.25°) in the incident beam path and a fixed anti-scatter slit (0.25°) in the diffracted beam path were applied. One scan was performed during 1 h in the 2Θ range from 5° to 65°. Quantification of the XRD results was obtained using the Rietveld algorithm in the open-source XRD and Rietveld refinement software *Profex* (version 4.3.4). During Rietveld refinement, the following parameters were refined: scale factor, sample displacement, background (Chebyshev polynomial function, 11 coefficients), crystallite size, microstrain, selected lattice parameters, and preferred orientation (spherical harmonics). The reference structures for all phases used in Rietveld refinements are given in Table 1.

2.5 | Compressive strength development

Two sets of experiments regarding the compressive strength development in the dependence of $Ca(NO_3)_2$ addition have been performed. In the first set of experiments, the compressive strength development was tested

TABLE 1 Crystallography Open Database (COD) ID and reference of all phases used in Rietveld refinements of anhydrous and hydrated cement samples

Phase	COD-ID	Reference
Alite	9008366	[38]
Belite	1546027	[39]
C_3A (cubic)	1000039	[40]
C_3A (orthorhombic)	9014308	[41]
Brownmillerite	1200009	[42]
Periclase	1000053	[43]
Calcite	9000965	[44]
Arcanite	9007569	[45]
Gypsum	2300259	[46]
Bassanite	2105042	[47]
Anhydrite	5000040	[48]
Portlandite	1001768	[49]
Ettringite	9015084	[50]
CO_3-AFm (mono)	1000459	[51]
CO_3-AFm (hemi)	2105252	[52]
NO_3-AFm	2008643	[23]
Rutile	9015662	[53]

on 2-cm cubes prepared from cement paste, as described in Section 2.2. Each compressive strength value presented in Section 3 represents the average result of 10 tested cubes. In the second set of experiments, the compressive strength development was tested on mortar prisms according to EN 196-1[35] to allow direct comparison of the presented results with comparable experimental data available in the literature. The compressive strength was tested after 1, 7, and 28 days of hydration. All samples for compressive strength testing were removed from their molds 24 h after preparation. Until testing, samples were stored under water at 20°C.

2.6 | Pore solution analysis

Pore solutions were analyzed by ICP-OES (IRIS Intrepid II XSP, Thermo Fisher, USA). Samples for ICP-OES analysis were prepared at a *w/c* of 1 to facilitate the extraction of pore solution via centrifugation.

Pore solution was extracted from samples via centrifugation for 10 min at 1195 g after defined hydration times. After centrifugation, the pore solution was filtered through a 450-nm polyester filter to remove any remaining solids. After filtration, 4 g of the filtered pore solution was diluted with 16 g of ultrapure water (σ = 0.06 μS/cm). The samples were acidified with HNO_3 to pH 2 immediately after dilution.

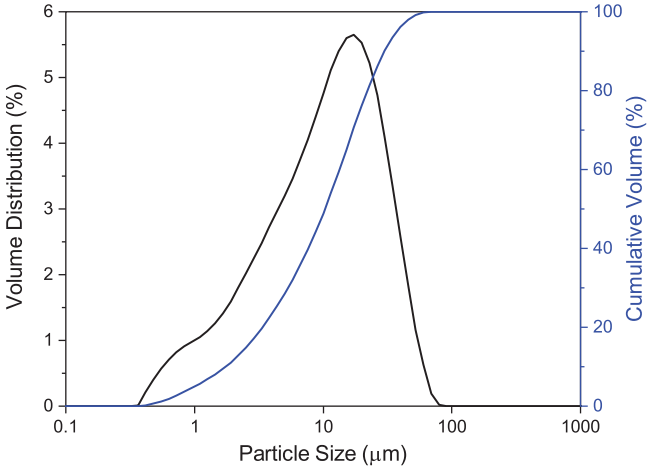

FIGURE 1 Particle size distribution of the analyzed cement determined by laser diffraction analysis

2.7 | Thermodynamic calculations

The thermodynamic modeling was performed by Gibbs energy minimization using the software package GEMS[54,55] in version 3.5 equipped with the databases PSI-Nagra 12/07[56] and Cemdata18.[57] This approach was used to model the phase assemblage at full hydration and estimate the pseudo-equilibria resulting from the initially dissolving phases, both depending on the added quantity of $Ca(NO_3)_2$. All calculations were performed for 20°C.

3 | RESULTS

3.1 | Raw materials characterization

The particle size distribution of the analyzed cement (CEM I 52.5 R) was measured using laser diffraction analysis (Mastersizer 2000, Malvern Panalytical, United Kingdom) and is presented in Figure 1. The analyzed cement has a specific surface of 4700 ± 100 cm^2/g, determined by the Blaine method according to EN 196-6.[58] The chemical composition of the cement was determined by X-ray fluorescence (WD-RFA PW 2400, Phillips, the Netherlands) and is given in Table 2. The mineralogical composition of the cement was determined through the Rietveld refinement of XRD results and is presented in Table 3.

3.2 | Isothermal heat flow calorimetry

Isothermal heat flow calorimetry is a frequently applied technique in the analysis of cement hydration and the effect of cement additives on the hydration as it allows to follow the heat production rate (heat flow) over time.

TABLE 2 Chemical composition of the analyzed cement determined by X-ray fluorescence (XRF)

	Al_2O_3	CaO	Fe_2O_3	K_2O	MgO	MnO	Na_2O	P_2O_5	SiO_2	SO_3	TiO_2	LOI	Sum
wt.%	4.9	62.5	3.0	1.2	2.2	0.1	0.3	0.1	19.2	3.3	0.2	2.5	99.1

TABLE 3 Mineral composition of the analyzed cement determined by the Rietveld refinement of X-ray diffraction (XRD) data

Phase	wt.%
Alite	66
Belite	5
C_3A (cubic)	2
C_3A (orthorhombic)	5
Brownmillerite	11
Periclase	<1
Calcite	4
Arcanite	2
Gypsum	<1
Bassanite	1
Anhydrite	3

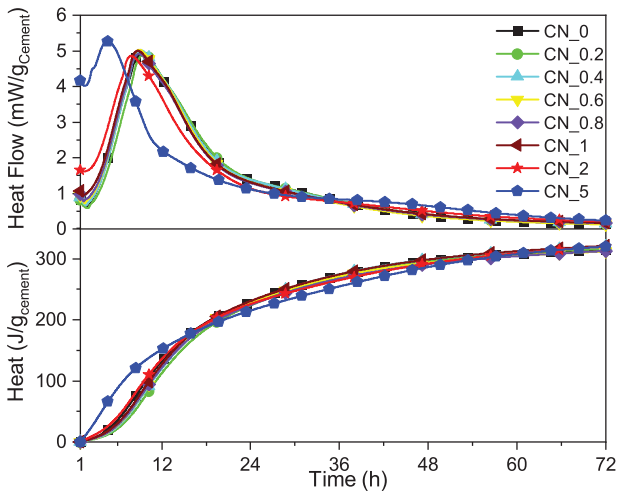

FIGURE 2 Heat flow and heat development of the tested cement pastes ($w/c = 0.5$) determined by isothermal heat flow calorimetry. The heat flow during the first hour of hydration was excluded from the calculation of the cumulative heat

The results of isothermal heat flow calorimetry (Figure 2) indicate that $Ca(NO_3)_2$ dosages <0.8 wt.% of cement only have a minor influence on cement hydration during the first 72 h of hydration. $Ca(NO_3)_2$ dosages ≥1 wt.%, however, reduce the duration of the induction period. Accordingly, the onset of the acceleration period and the heat flow maximum ascribed to the main hydration of alite is shifted to earlier times by increasing $Ca(NO_3)_2$ dosages. For example, at a $Ca(NO_3)_2$ dosage of 5 wt.% of cement, the heat flow maximum occurs at 276 min and, thus, 270 min earlier than in the neat reference sample. Further, $Ca(NO_3)_2$ dosages >1 wt.% increase heat flow measured during the induction period. At an addition of 5 wt.% $Ca(NO_3)_2$ also, the heat flow measured at the heat flow maximum is increased. For $Ca(NO_3)_2$ additions ≥1 wt.%, the cumulative heat of hydration is slightly increased in the presence of $Ca(NO_3)_2$ until ~12 h of hydration but is not increased after 72 h of hydration. The results of the heat flow calorimetry measurements performed with w/c of 1 (Figure S1), which corresponds to the sample composition chosen for pore solution analysis, show corresponding trends.

3.3 | In situ XRD and QXRD

In situ XRD is a technique frequently applied in the analysis of construction materials to study the consumption of cement phases and the formation of crystalline hydration products, such as ettringite and portlandite. The XRD reflex intensity development of the samples CN_0, CN_2, and CN_5, measured by in situ XRD over 24 h, is shown in Figure 3. As identical measurement settings were chosen for each sample, the reflex intensity developments of the three samples can be compared. The results show a reduction in the time that passes until the intensity of the alite reflex decreases, and the CH reflex intensity starts to rise earlier as the $Ca(NO_3)_2$ addition was increased. This indicates an early onset of the alite hydration and an early formation of CH and C–S–H, respectively, which correlates well with the shift of the heat flow maximum to earlier times with increasing $Ca(NO_3)_2$ additions observed in isothermal calorimetry. The rate of C_3A dissolution appears not to be affected by the presence of $Ca(NO_3)_2$ in solution during the first 6–8 h of hydration, which is in-line with the results of Ye et al.[59] The initially observed gypsum reflex intensities in samples CN_2 and CN_5 are increased compared to sample CN_0. However, the intensity development of gypsum suggests that the dissolution of gypsum occurs at an earlier time and at a higher rate in the presence of increasing amounts of $Ca(NO_3)_2$, resulting in an earlier gypsum depletion. Depletion of gypsum occurs after ~8 h in sample CN_0, after 7 h in sample CN_2 and after 3 h in sample CN_5. Anhydrite is also consumed faster in the presence of $Ca(NO_3)_2$ according to the reflex intensity development. Parallel to the increased dissolution of gypsum and anhydrite, the rate of ettringite

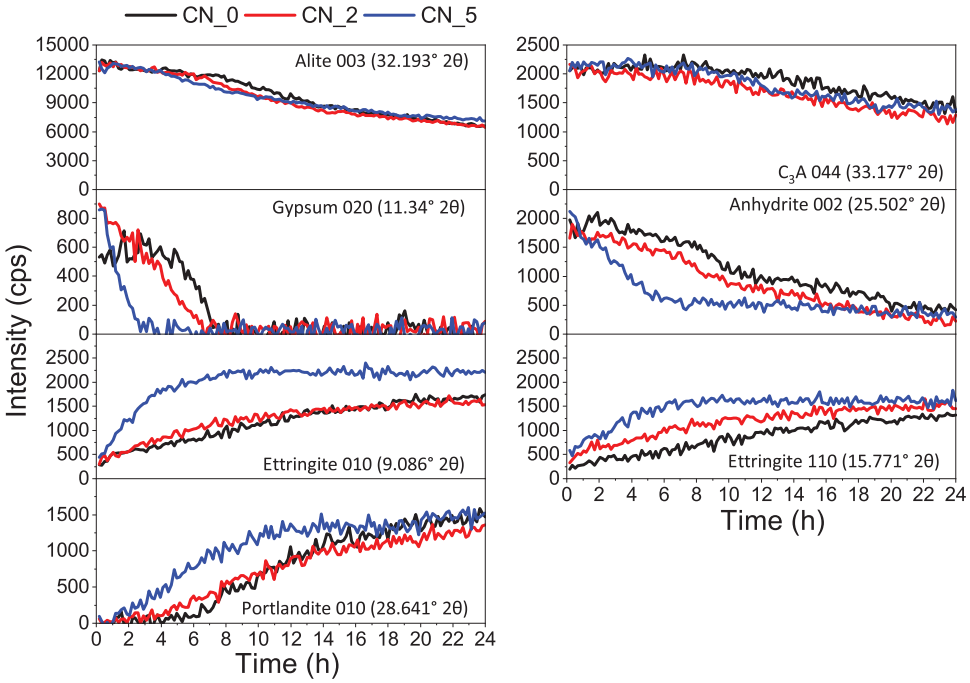

FIGURE 3 Reflex intensity development of several cement phases and hydration products determined by in situ X-ray diffraction (XRD) analysis of hydrating cement pastes

formation is increased, especially at the high $Ca(NO_3)_2$ dosage of 5 wt.%, as indicated by the fast increase of the ettringite reflex intensities.

Because of the high scan speed and the initially low crystallinity of AFm phases (including SO_4-AFm and strätlingite as well as NO_3-AFm and CO_3-AFm (mono and hemi)), peak intensities of AFm phases are too low to analyze the development of these phases using in situ XRD during the first 24 h of hydration.

The quantification of XRD results using the Rietveld algorithm is a frequently applied technique to obtain quantitative information on the phase composition of a hydrated cement sample after a defined period of hydration. In the present study, the quantification of XRD results was performed on samples hydrated for 1, 7, and 28 days. The results after 1 day of hydration indicate the hydrated cement phase composition at the end of the in situ XRD measurement. Rietveld refinement results of cement hydrated for 7 and 28 days reflect the cement phase composition at later stages of hydration. The pattern of sample CN_0 hydrated for 1 day, refined by the Rietveld algorithm, is shown in Figure 4, representing the refined patterns leading to the QXRD results summarized in Figure 7. Figure 5 shows the complete range of all diffractograms used for the quantitative determination of the phase composition, whereas Figure 6 focuses on the 2Θ range between 5° and 17° 2Θ, in which the highest intensity reflexes of the hydration products of the aluminate reaction appear.

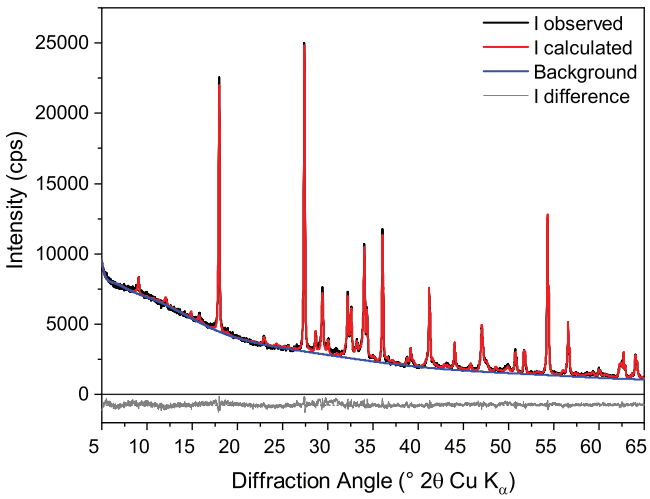

FIGURE 4 Representative Rietveld refinement pattern of sample CN_0 hydrated for 1 day. The difference between the observed and the calculated intensities is plotted below the diagram

At the end of the in situ measurement, after 24 h of hydration, QXRD results reveal that the remaining amounts of the clinker minerals alite, belite, C_3A and C_4AF are, within small margins, comparable in all analyzed samples with a maximum difference between the individual samples of ~2 wt.% for alite and below 1 wt.% for belite, C_3A and C_4AF (Figure 7). Thus, although $Ca(NO_3)_2$ influences the rate of hydration initially, the progress of

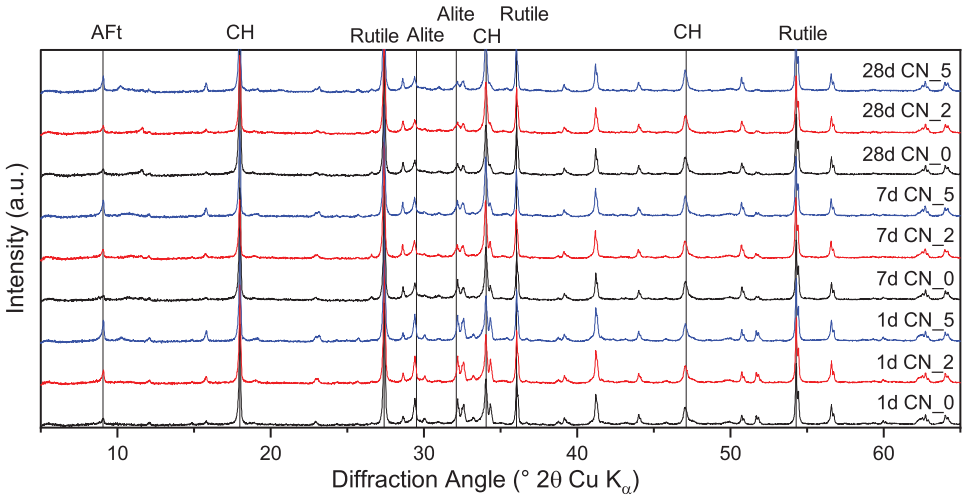

FIGURE 5 Complete diffractograms of cement pastes hydrated for 1, 7, and 28 days in the presence of 0-, 2-, and 5 wt.% $Ca(NO_3)_2$. To facilitate the interpretation, the background has been subtracted. The reflexes of the hydration products ettringite (AFt), portlandite (CH), alite, and the internal standard rutile (TiO_2) are highlighted by droplines

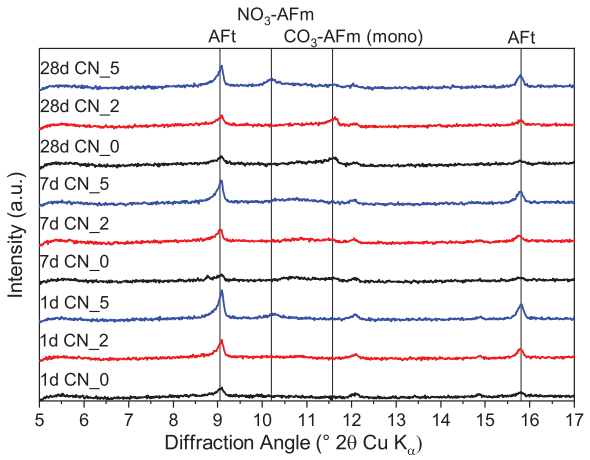

FIGURE 6 Diffractograms of cement pastes hydrated for 1, 7, and 28 days in the presence of 0-, 2- and 5 wt.% $Ca(NO_3)_2$ in the range from 5° to 17° 2Θ. The reflexes of the hydration products ettringite (AFt), NO_3-AFm, and CO_3-AFm (mono) are highlighted by droplines

hydration later than 24 h appears to be independent of $Ca(NO_3)_2$ addition.

Regarding the crystalline hydration products, the addition of $Ca(NO_3)_2$ leads to a significant increase in the content of ettringite in the hydrated cement. After 24 h of hydration, 3 wt.% ettringite were determined in the reference sample, whereas 7 and 9 wt.% were determined in samples CN_2 and CN_5, respectively. Further, 2 wt.% NO_3-AFm were determined in sample CN_5 after 24 h of hydration. Moreover, after 7 and 28 days of hydration, amounts of NO_3-AFm >1 wt.% were determined in sample CN_5 at both ages. At 28 days of hydration, the amount of CO_3-containing AFm phases was reduced from 4 wt.% in sample CN_0 to 3 wt.% in sample CN_5 (Figure 7).

3.4 | Compressive strength development

The evaluation of compressive strength at different hydration times is a widely applied method to follow the hardening of cement pastes and mortars. The results of compressive strength testing are summarized in Figure 8. The 1-day compressive strength of the 2-cm cubes made from cement paste is slightly increased in the presence of 1 wt.% $Ca(NO_3)_2$ from 28.1 to 30.2 N/mm^2. However, 5 wt.% $Ca(NO_3)_2$ reduces the 1-day compressive strength of the tested paste cubes to 21 N/mm^2. After 7 and 28 days of hydration, all $Ca(NO_3)_2$ containing samples show higher compressive strengths than the reference samples. With 57.3 N/mm^2, the highest paste cube compressive strength has been determined for sample CN_2 after 28 days of hydration. On average, the 28-day paste cube compressive strength is increased by ~13 % in the presence of $Ca(NO_3)_2$ compared to reference sample.

Regarding the compressive strength development of the mortar prisms, similar trends have been observed as for the 2-cm paste cubes (Figure 8). In the presence of $Ca(NO_3)_2$ dosages exceeding 1 wt.%, the 1-day mortar prism compressive strength is slightly reduced compared to the reference sample. However, the observed effect of $Ca(NO_3)_2$ on the compressive strength development of mortar prisms is significantly less pronounced as for the 2-cm paste cubes. Especially after 28 days of hydration, the differences between the tested samples are within the variance of the results so that no significant influence of

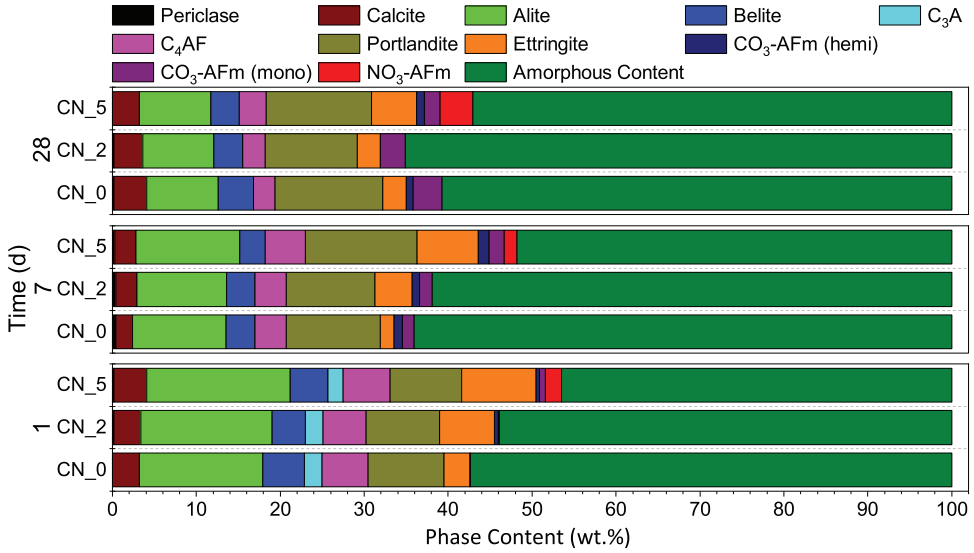

FIGURE 7 Phase composition of cement hydrated for 1, 7, and 28 days in dependence of $Ca(NO_3)_2$ addition determined by quantitative X-ray diffraction (QXRD)

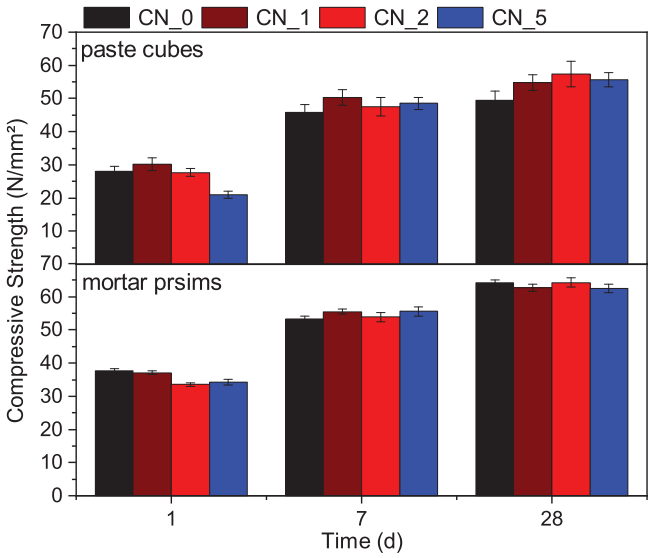

FIGURE 8 Compressive strength development of paste cubes and mortar prisms in dependence of $Ca(NO_3)_2$ addition

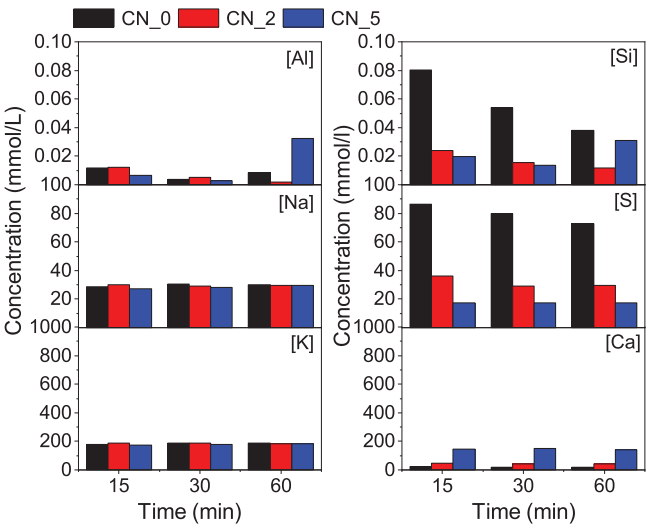

FIGURE 9 Ion concentrations in pore solutions extracted by centrifugation of 10 min after 5, 20, and 50 min of undisturbed hydration in dependence of $Ca(NO_3)_2$ addition

$Ca(NO_3)_2$ on the 28 days compressive strength could be determined.

3.5 | Pore solution analysis

The analysis of the pore solution by ICP-OES is a method that, by revealing the ion concentrations in the pore solution at specific times of hydration, offers valuable insights into the chemical processes of cement hydration. As seen in the former sections, the addition of $Ca(NO_3)_2$ influences most significantly the early reaction rate. To investigate this early influence further, pore solution was collected after 5, 20, and 50 min of undisturbed hydration, after which the samples were centrifuged for 10 min to separate the pore solution from the solids. The results in Figure 9 show that [Ca] during the first 60 min of hydration stays on a comparably constant level of ~20 mmol/L in sample CN_0 and ~45 and 145 mmol/L in samples CN_2 and CN_5, respectively. [S] is steadily declining in all samples during the first 60 min of hydration and is reduced in the presence of $Ca(NO_3)_2$, from ~86 mmol/L in sample CN_0 after 15 min of hydration to ~17 mmol/L in sample CN_5 at the same time. [Si] is reduced in the

presence of $Ca(NO_3)_2$ from 80 μmol/L in sample CN_0 to ~20 μmol/L in the samples CN_2 and CN_5 after 15 min of hydration. Furthermore, [Si] slightly decreases between 30 and 60 min of hydration in the samples CN_0 and CN_2, whereas it slightly increases in the sample CN_5 during the same period. Moreover, [Al] is reduced from 11.6 μmol/L in sample CN_0 to 8.5 μmol/L in sample CN_5 after 15 min of hydration. After 60 min of hydration, the sample CN_5 shows the highest [Al] in the pore solution.

3.6 | Thermodynamic calculations

Thermodynamic modeling is classically used to estimate the phase assemblage in thermodynamic equilibrium of a chemical system. In the context of inorganic binders, this means the phase assemblage after an infinitely long hydration time. Nevertheless, the dissolved quantity of each precursor phase at a given point of time can be used to estimate the kind and quantity of precipitates and the ion concentrations in the pore solution as a function of time.[60–62] This approach has successfully been used to model the evolution of solids and liquid phase composition in Portland cements starting at a few minutes of hydration.[60–62] In the current work, thermodynamic calculations for the pseudo-equilibrium during the initial dissolution and at complete hydration are performed depending on the $Ca(NO_3)_2$ addition.

For the pseudo-equilibria, during initial dissolution, it was assumed that of the calcium sulfates in the cement, only bassanite dissolves completely during the first minutes of cement hydration.[63] Further, the initial dissolution of 1.8-g C_3A per 100 g of cement[64] and the complete dissolution of arcanite[63] were assumed for this calculation. As the ionic concentrations measurement indicate the presence of silicon and some sodium (Figure 9), the dissolution of 0.1 g of C_3S was assumed and 0.05-g Na_2O was added as well to the starting parameters of the calculation. The precipitation of gibbsite and microcrystalline $Al(OH)_3$ was suppressed, as these phases cannot form in the timeframe of interest.[65] Figures 10 and 11 show the thermodynamically predicted hydration products and element concentrations in the pore solution, calculated based on the initial dissolution of cement phases in dependence of the $Ca(NO_3)_2$ addition. These calculations are intended as an indicator for the development of the system. It is unlikely that the system will ultimately reach the calculated (pseudo-)equilibrium states, and mutual kinetic influences between the phases are not possible to account for. Nevertheless, the calculations can be used to see in which direction the need of minimizing the Gibbs free energy will force the system.

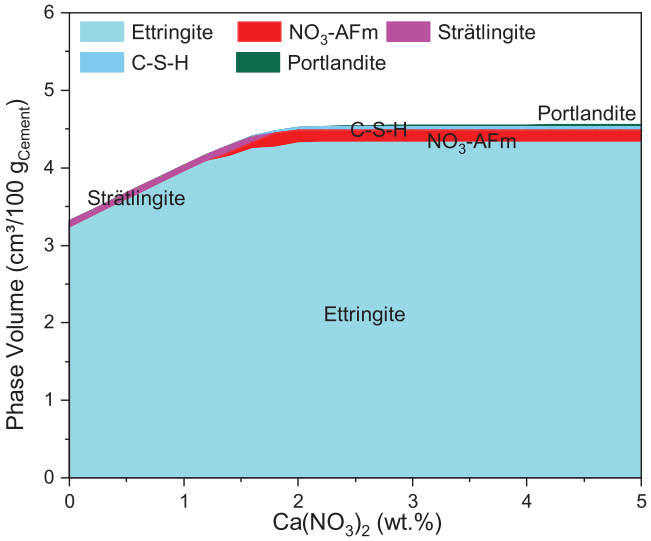

FIGURE 10 Thermodynamically calculated hydration products based on the pseudo-equilibria of the initially dissolved phases in dependence of $Ca(NO_3)_2$ addition

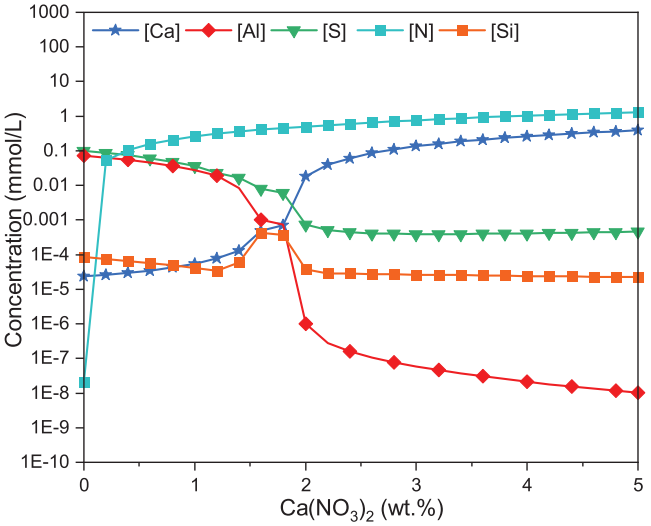

FIGURE 11 Thermodynamically calculated ion concentrations in solution based on the pseudo-equilibria of the initially dissolved phases in dependence of $Ca(NO_3)_2$ addition

Thermodynamic modeling predicts a substantial increase of the initially forming ettringite quantity for increasing $Ca(NO_3)_2$ additions, which can be verified by in situ XRD (Figure 3). In contrast, the predicted development of AFm phases (NO_3-AFm and strätlingite) cannot be detected by in situ XRD, which is likely explained by the low crystallinity of early forming AFm phases.

The thermodynamic prediction of the ion concentrations in the pore solution correlates well with the trends revealed by pore solution analysis (Figure 9). Calculated and measured ion concentrations indicate that [Ca] rises with increasing $Ca(NO_3)_2$ additions, whereas

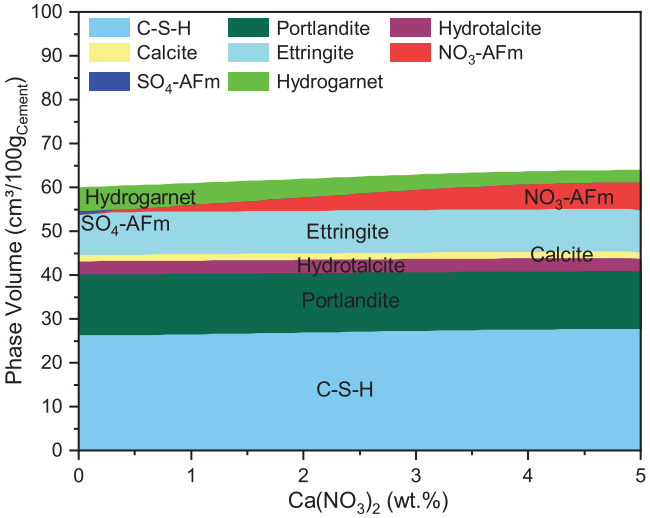

FIGURE 12 Calculated phase composition of the fully hydrated cement (assuming calcite as inert) in dependence of the $Ca(NO_3)_2$ addition relative to cement mass

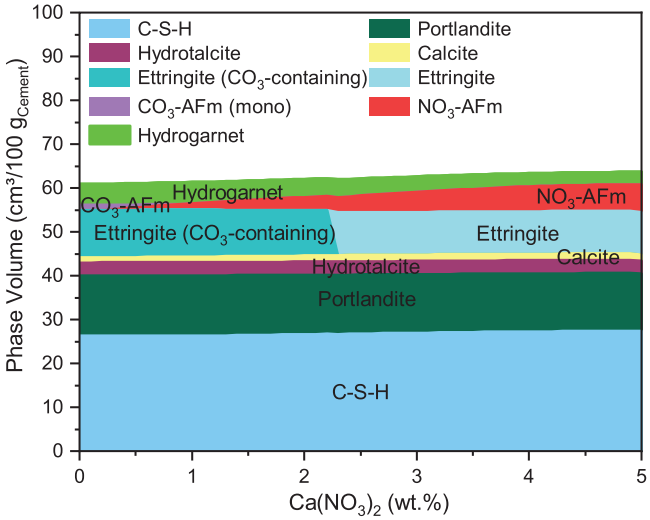

FIGURE 13 Calculated phase composition of the fully hydrated cement (assuming calcite as reactive) in dependence of the $Ca(NO_3)_2$ addition relative to cement mass. The formation of thaumasite was suppressed for the calculation

the alkali concentrations remain nearly constant. The slightly decreasing trend predicted for [Si] (except a rise at ~1.75 wt.% $Ca(NO_3)_2$) was also confirmed by the results of pore solution analysis as well as the decline of [S] and [Al], predicted for increasing $Ca(NO_3)_2$ additions. Furthermore, [N] has been predicted to increase sharply at low $Ca(NO_3)_2$ additions. Especially the decline of [Al] might be particularly interesting for the acceleration of cement hydration by $Ca(NO_3)_2$ and will be recalled in the following discussion.

For the total hydration of the cement, two cases were assumed: no participation of calcium carbonate in the reaction and full participation of calcium carbonate. These two cases were considered as calcium carbonate may participate slower in the reaction than the clinker phases.[61,63] Consequently, the experimentally observed phase assemblage should be comparable to a state in-between these two models. In the performed calculations, the formation of goethite and hematite was suppressed, as these phases are stable at room temperature but do not form within a reasonable time due to kinetic hindrances.[65,66]

Figure 12 shows the thermodynamically calculated hydrate assemblage of the fully hydrated cement in dependence of the $Ca(NO_3)_2$ addition, assuming no participation of calcium carbonate. The results suggest that the volume of ettringite increases slightly at the expense of OH-containing SO_4-AFm for small $Ca(NO_3)_2$ additions but stay unchanged for $Ca(NO_3)_2$ additions exceeding 0.5 wt.%. Furthermore, the volume of C–S–H increases slightly but continuously with increasing $Ca(NO_3)_2$ additions. The volume of NO_3-AFm increases significantly with increasing $Ca(NO_3)_2$ additions, partially at the expense of the Fe–Si-containing hydrogarnet, the volume of which slightly declines. The volumes of portlandite and OH-hydrotalcite stay constant over the entire $Ca(NO_3)_2$ addition range from 0 to 5 wt.%.

The enhanced formation of NO_3-AFm and, to a smaller extent, ettringite and C–S–H in the presence of $Ca(NO_3)_2$ leads to an increase of the solid phase volume in the fully hydrated cement of ~4 cm^3/100 g of cement at an addition of 5 wt.% $Ca(NO_3)_2$. This mechanism is comparable to the volume increase by $CaCO_3$ addition, which leads to a replacement of SO_4-AFm by CO_3-AFm phases and ettringite.[61,65,67]

When the full participation of calcite is assumed, the modeling results are comparable in many points, but the formation of thaumasite is predicted at high $Ca(NO_3)_2$ additions (Figure S2). Nevertheless, thaumasite was observed in none of the current samples. A potential reason for this discrepancy may be that thaumasite formation commonly occurs only at temperatures <15°C (ideally 0–5°C)[68,69] and is very slow,[70,71] although thaumasite may be stable also at an elevated temperature depending on the system.[65,72] As no thaumasite was detected in XRD, the formation of thaumasite was suppressed for the thermodynamic calculation of the results presented in Figure 13. In this case, ettringite is CO_3-containing at low $Ca(NO_3)_2$ additions, and its quantity decreases slightly over the whole $Ca(NO_3)_2$-addition range, as it was also observed for portlandite and Fe,Si-containing hydrogarnet. C–S–H and calcite increase slightly, whereas NO_3-AFm increases strongly with increasing $Ca(NO_3)_2$ additions. CO_3-AFm (mono) is formed only at low $Ca(NO_3)_2$ additions, whereas calcite is a part of the equilibrium phase assemblage over the whole analyzed $Ca(NO_3)_2$ concentration range. The

overall volume of solid phases increases over the whole range of $Ca(NO_3)_2$ additions, as it was also found for the assumption of complete non-reactivity of calcite.

Several discrepancies between the thermodynamically calculated results and the measured results of QXRD must be addressed. No CO_3-AFm is predicted by thermodynamics for samples containing ≥0.5 wt.% $Ca(NO_3)_2$ whereas QXRD results show the formation of up to 2 wt.% CO_3-AFm (mono) in sample CN_5 after 28 days, which might indicate the carbonation of QXRD samples. Furthermore, no hydrogarnet could be detected by XRD analysis. However, Dilnesa et al.[66] showed that hydrogarnet is the dominating Fe-containing phase in hydrated OPCs. According to their study, hydrogarnet is difficult to detect by standard analytical techniques, such as XRD of nonselectively dissolved samples, which might explain why it was not detected in QXRD analysis.

4 | DISCUSSION

Isothermal heat flow calorimetry, in situ XRD, and the pore solution analysis indicate significant influences of $Ca(NO_3)_2$ on the early cement hydration. The increased heat flow during the induction period in the presence of $Ca(NO_3)_2$, measured by isothermal calorimetry, indicates an increased reactivity at this early stage of hydration. The processes responsible for this increased reactivity are revealed by in situ XRD and pore solution analysis and corroboration of the results by thermodynamic calculations.

In situ XRD shows that the initial gypsum reflex intensities are significantly higher in the presence of $Ca(NO_3)_2$ as compared to the neat reference sample CN_0. On the one hand, this observation might indicate that the presence of $Ca(NO_3)_2$ depresses the dissolution of gypsum and that, during the 8 min of sample preparation for in situ XRD, a fast initial dissolution of gypsum occurred only in the neat reference sample. On the other hand, the observed increased gypsum reflex intensities might indicate that $Ca(NO_3)_2$ enforces a rapid precipitation of additional gypsum by increasing the availability of calcium in solution. Jansen et al.,[73] who analyzed the early hydration of an additive-free cement paste by quantification of in situ XRD results, found that in their cement paste, no rapid reaction of gypsum occurred during the first 4 h of hydration. Based on this observation by Jansen et al.,[73] it was assumed that fast precipitation of gypsum occurred during the initial minutes of hydration in the $Ca(NO_3)_2$ containing samples CN_2 and CN_5. Moreover, Justnes et al.[19] assumed that the fast precipitation of gypsum might occur in hydrating $Ca(NO_3)_2$-containing cement pastes. The sulfate required for this initial gypsum precipitation presumably originates from the fast dissolving alkali-sulfate arcanite,[19] of which the analyzed cement contains 2 wt.% according to QXRD, as well as the initial dissolution of bassanite. The depressed sulfate concentration during the first 60 min of hydration in the presence of $Ca(NO_3)_2$, measured by ICP-OES, supports the assumption of initial gypsum precipitation. Although Justnes et al.[19] assumed that the precipitation of gypsum would slow the formation of ettringite due to a scarce solubility of gypsum, the opposite is found to occur in the present study.

Although the reflex intensity of gypsum (measured by in situ XRD) stays on an approx. constant level during the first 4 h of hydration in the neat cement paste CN_0, gypsum reflex intensities measured for CN_2 and CN_5 immediately start to decline, suggesting a fast dissolution of the initially precipitated gypsum. Moreover, the rate of anhydrite dissolution increases during the first hours of cement hydration, whereas the rate of C_3A dissolution appears to be unaffected during the first 8 h of hydration in the presence of $Ca(NO_3)_2$.

As the increased dissolution of cement phases enforces increased precipitation of hydration products, parallel to the fast dissolution of gypsum and anhydrite, ettringite is precipitated at a higher rate in samples CN_2 and CN_5 as compared to sample CN_0. As discussed earlier, due to their low initial crystallinity, the formation of AFm phases could not be observed in in situ XRD. However, besides the increased ettringite formation, QXRD of the dried samples showed that NO_3-AFm had been formed in sample CN_5 during the first 24 h of hydration, and that the determined amount of NO_3-AFm in sample CN_5 further increased to 4 wt.% after 28 days of hydration.

Thermodynamic modeling of the initial phase composition and the phase composition in the fully hydrated cement corroborate the presented measurement results regarding the effect of $Ca(NO_3)_2$ on the formation of aluminate-containing hydration products during the hydration of a commercial OPC. Both the initial formation of an increasing amount of ettringite and the formation of NO_3-AFm, at the expense of SO_4-AFm or CO_3-AFm, due to increasing additions of $Ca(NO_3)_2$, were indicated by the results of the thermodynamic calculations, which is in-line with the results of Balonis et al.[14]

Besides a heat flow increase during the induction period, isothermal heat flow calorimetry (Figure 2) shows, for increasing $Ca(NO_3)_2$ additions, a reduction of the time that passes until the heat flow maximum is reached. This suggests an acceleration of alite hydration, which is most significant for the highest analyzed $Ca(NO_3)_2$ dosage of 5 wt.% in sample CN_5. In situ XRD confirms this acceleration of alite hydration in the presence of $Ca(NO_3)_2$ as indicated by the early onset of alite reflex intensity decrease and portlandite reflex intensity increase (Figure 3).

The increased calcium concentration in the pore solution is regularly discussed as the primary cause for the acceleration of alite hydration in the presence of $Ca(NO_3)_2$.[18,26] However, the present study results suggest that the effect of $Ca(NO_3)_2$ on the aluminate concentration in solution might also contribute to the observed acceleration of alite hydration.

The presence of $Ca(NO_3)_2$ increases, as discussed earlier, the formation of the aluminum-containing hydration products ettringite and NO_3-AFm, whereas the dissolution of C_3A appears to be unaffected during the initial period of hydration. Consequently, a decrease of [Al] in the initial pore solution was expected and the thermodynamic calculations, based on the pseudo-equilibria of the initially dissolving phases, indicated the described reduction of [Al] in the initial pore solution for increasing $Ca(NO_3)_2$ concentrations.

Moreover, the analysis of the pore solution composition by ICP-OES showed a reduction of the [Al] from 11.6 μmol/L in sample CN_0 to 6.4 μmol/L in sample CN_5 in early pore solution composition after 15 min of hydration. CN_5 also has after 30 min still the lowest [Al]. After 60 min of hydration, however, the highest aluminum concentration in the pore solution was measured in sample CN_5 with 32.6 μmol/L, which might be attributed to a further progressed state of hydration of the sample CN_5 at that time and the onset of aluminum release from dissolving alite.[63] However, it must be considered that the measured [Al] concentrations are very low, even though they are well above the limit of quantitation of 0.07 μmol/L, and that minor and unavoidable deviations in sample preparation might influence the pore solution composition at such low concentrations.

Nevertheless, based on the results of thermodynamic calculations and the indications of pore solution analysis, the addition of $Ca(NO_3)_2$ can lead to a reduction of aluminum concentration in pore solution, which might contribute to the observed early onset of alite hydration. The mechanism causing the retarding effect of aluminum on the alite hydration has not yet been fully resolved and could not be further investigated in the present study. Begarin et al.[74] proposed that in the presence of aluminum, the formations of C–A–S–H nuclei, which are not acting as seeds for further C–S–H growth, are responsible for the retarded onset of fast alite hydration. Nicoleau et al.[27] and Pustovgar et al.[75] were, however, able to show that it is rather a poisoning of the alite surface by aluminum that inhibits alite dissolution in the presence of aluminum.

Regarding the compressive strength development, $Ca(NO_3)_2$ slightly reduces the compressive strength measured after 1 day of hydration and enhances the compressive strength measured after 7 and 28 days of hydration, which has also been reported in literature.[17,76,77] According to Oey et al.,[17] the slight reduction of 1-day compressive strength in $Ca(NO_3)_2$-accelerated samples might originate from a rapid decrease of clinker particle surfaces in direct contact with the pore solution, due to the initially increased rate of hydration product formation. After the hydration maximum, the rate of hydration in the accelerated samples decreases faster than in the unaccelerated samples. After ≥24 h, the hydration in accelerated and unaccelerated samples continues at a moderate rate, and QXRD results after 7 and 28 days show that the amount of remaining clinker phases is comparable in samples CN_0, CN_2, and CN_5. This indicates that the progress of hydration is independent of the $Ca(NO_3)_2$ addition after the initial hours of hydration. The thermodynamic calculation of the phase composition of the fully hydrated cement (Figures 12 and 13) shows that $Ca(NO_3)_2$ increases the total phase volume of the hydrated cement. The reason for that is the formation of NO_3-AFm and to a significantly smaller amount also the increase of C–S–H as well as, depending on the assumed $CaCO_3$ reactivity, ettringite. This observation suggests that the increase in the total phase volume and the denser structure of the hydrated cement[61,62] leads to the increase in compressive strength in $Ca(NO_3)_2$-accelerated samples observed on the tested cement paste cubes after 7 and 28 days of hydration. The influence of $Ca(NO_3)_2$ on the compressive strength development was significantly less pronounced for the mortar prisms made according to EN 196-1[35] compared to the 2 cm cubes made from cement paste. No weakening effect of $Ca(NO_3)_2$ on the interfacial transition zone between aggregates and hardened cement paste has been reported in the literature. Consequently, the enhanced effect of $Ca(NO_3)_2$ on the tested paste cubes might be explained by the fact that the volume share of the sample affected by $Ca(NO_3)_2$ is higher in the paste cubes, which do not contain sand, as in the sand containing mortar prisms.

5 | CONCLUSIONS

The presented results were obtained by analyzing one commercial CEM I 52.5 R in a series of experiments and thermodynamic calculations. The experimental results and the results of the thermodynamic calculations indicate that $Ca(NO_3)_2$ accelerates the silicate reaction of a hydrating OPC paste and significantly influences the initial formation of AFm phases and ettringite. In the presence of $Ca(NO_3)_2$, fast initial precipitation of gypsum occurs. This initially precipitated gypsum then quickly dissolves at a higher rate than the gypsum present in the neat reference sample. Moreover, the dissolution of anhydrite has been enhanced in the presence of $Ca(NO_3)_2$.

Besides the increased dissolution rate of the two calcium sulfates, gypsum and anhydrite, the ettringite formation is enhanced, especially at the highest analyzed dosage of 5 wt.% $Ca(NO_3)_2$. Furthermore, significant amounts of NO_3-AFm are formed in the presence of $Ca(NO_3)_2$. No indications for an increased rate of C_3A dissolution in the presence of $Ca(NO_3)_2$ were found during the initial 8 h of hydration. Regarding the silicate reaction, it could be shown that $Ca(NO_3)_2$ decreases the time that passes until the fast alite hydration starts. Based on the thermodynamic calculation of the initial pore solution composition as well as the analysis of early pore solution composition by ICP-OES, it appears that besides a significant increase in [Ca], a decrease in the [Al] in pore solution might contribute to the acceleration of alite hydration in the presence of $Ca(NO_3)_2$.

ACKNOWLEDGMENTS

The authors acknowledge Thomas Matschei for fruitful discussions in the context of this publication. Furthermore, the authors want to thank the assigned reviewers for their constructive criticism, which helped us to improve the quality of our manuscript. This work was funded by the German Federal Ministry of Education and Research in the scope of the project BauProAddi (FKZ: 03XP0122A).

Open access funding enabled and organized by Projekt DEAL.

ORCID

Tobias Dorn https://orcid.org/0000-0001-6431-1199
Tamino Hirsch https://orcid.org/0000-0002-0938-4261
Dietmar Stephan https://orcid.org/0000-0002-1893-6785

REFERENCES

1. Myrdal R. Sintef Report – accelerating admixtures for concrete: state of the art (978-82-536-0989-8). 2007. p. 1–35. Accessed June 13, 2018.
2. Escalante-García J, Sharp J. Effect of temperature on the hydration of the main clinker phases in Portland cements: Part I, Neat cements. Cem Concr Res. 1998;28:1245–57.
3. Escalante-Garcıá JI, Sharp JH. Effect of temperature on the hydration of the main clinker phases in Portland cements: Part II, Blended cements. Cem Concr Res. 1998;28:1259–74.
4. Liu Z, Sha A, Hu L, Lu Y, Jiao W, Tong Z, et al. Kinetic and thermodynamic modeling of Portland cement hydration at low temperatures. Chem Pap. 2017;71:741–51.
5. Biernacki JJ, Bullard JW, Sant G, Banthia N, Brown K, Glasser P, et al. Cements in the 21st century: challenges, perspectives, and opportunities. J Am Ceram Soc. 2017;100:2746–73.
6. Rehman AU, Kim J-H. 3D concrete printing: a systematic review of rheology, mix designs, mechanical, microstructural, and durability characteristics. Materials (Basel). 2021;14:3800.
7. Tao Y, Rahul AV, Lesage K, Yuan Y, van Tittelboom K, Schutter GD, et al. Stiffening control of cement-based materials using accelerators in inline mixing processes: possibilities and challenges. Cem Concr Compos. 2021;119:103972.
8. Esnault V, Labyad M, Chantin M, Toussaint F. Experience in online modification of rheology and strength acquisition of 3D printable mortars. In: Wangler T, Flatt RJ, editors. First RILEM international conference on concrete and digital fabrication – digital concrete. vol. 2019. Cham: Springer International Publishing; 2018. p. 24–38.
9. Tokar V. Additive composition for Portland cement materials, US 4,337,094. Euclid Chemical Co; 1981.
10. Kayyali OA, Haque MN. Chloride penetration and the ratio of Cl^-/OH^- in the pores of cement paste. Cem Concr Res. 1988;18:895–900.
11. Page CL, Short NR, Holden WR. The influence of different cements on chloride-induced corrosion of reinforcing steel. Cem Concr Res. 1986;16:79–86.
12. Abdelrazig B, Bonner D, Nowell DV, Dransfield J, Egan P. The solution chemistry and early hydration of ordinary Portland cement pastes with and without admixtures. Thermochim Acta. 1999;340–341:417–30.
13. Hill R, Daugherty K. The interaction of calcium nitrate and a Class C fly ash during hydration. Cem Concr Res. 1996;26:1131–43.
14. Balonis M, Mędala M, Glasser FP. Influence of calcium nitrate and nitrite on the constitution of AFm and AFt cement hydrates. Adv Cem Res. 2011;23:129–43.
15. Dorn T, Hirsch T, Stephan D. Study on the influence of accelerators on the hydration of Portland cement and their applicability in 3D printing. In: Mechtcherine V, Khayat K, Secrieru E, editors. Rheology and processing of construction materials: RheoCon2 & SCC9. Basingstoke, United Kingdom: Springer Nature; 2019.
16. Bost P, Regnier M, Horgnies M. Comparison of the accelerating effect of various additions on the early hydration of Portland cement. Constr Build Mater. 2016;113:290–6.
17. Oey T, Stoian J, Li J, Vong C, Balonis M. Comparison of $Ca(NO_3)_2$ and $CaCl_2$ admixtures on reaction, setting, and strength evolutions in plain and blended cementing formulations. J Mater Civ Eng. 2014;27:04014267.
18. Justnes H, Nygaard EC. Technical calcium nitrate as set accelerator for cement at low temperatures. Cem Concr Res. 1995;25:1766–74.
19. Justnes H, Nygaard EC. The mechanism of calcium nitrate as set accelerator for cement. In: Justnes H, editor. Proceedings of the 10th international congress on the chemistry of cement (ICCC), Gothenburg, Sweden, June 2–6. 1997. 3iii012 8pp.
20. Dorn T, Blask O, Stephan D. Acceleration of cement hydration – a review of the working mechanisms, effects on setting time, and compressive strength development of accelerating admixtures. Constr Build Mater. 2022;323:126554.
21. Franke W, Balonis M, Oey T, Sant G. The fate of nitrate ions in concrete under the focus of corrosion inhibition. In: 2nd international congress on durability of concrete, New Delhi, India, 4th–6th December 2014.
22. Renaudin G, Francois M, Evrard O. Order and disorder in the lamellar hydrated tetracalcium monocarboaluminate compound. Cem Concr Res. 1999;29:63–9.

23. Renaudin G, François M. The lamellar double-hydroxide (LDH) compound with composition $3CaO{\cdot}Al_2O_3{\cdot}Ca(NO_3)_2{\cdot}10H_2O$. Acta Cryst C. 1999;55:835–8.
24. Matschei T, Lothenbach B, Glasser FP. The AFm phase in Portland cement. Cem Concr Res. 2007;37:118–30.
25. Dorn T, Hirsch T, Stephan D. Analyzing the early structural build-up of accelerated cement pastes. Mater Struct. 2021;54:67.
26. Nicoleau L. Accelerated growth of calcium silicate hydrates: experiments and simulations. Cem Concr Res. 2011;41:1339–48.
27. Nicoleau L, Schreiner E, Nonat A. Ion-specific effects influencing the dissolution of tricalcium silicate. Cem Concr Res. 2014;59:118–38.
28. Quennoz A, Scrivener KL. Interactions between alite and C_3A-gypsum hydrations in model cements. Cem Concr Res. 2013;44:46–54.
29. Suraneni P, Flatt RJ. Use of micro-reactors to obtain new insights into the factors influencing tricalcium silicate dissolution. Cem Concr Res. 2015;78:208–15.
30. Odler I, Schüppstuhl J. Early hydration of tricalcium silicate III. Control of the induction period. Cem Concr Res. 1981;11:765–74.
31. Mota B, Matschei T, Scrivener KL. The influence of sodium salts and gypsum on alite hydration. Cem Concr Res. 2015;75:53–65.
32. Nehring J, Jansen D, Neubauer J, Goetz-Neunhoeffer F. Hydration of C_3S in presence of CA mineral-pore solution interaction. J Am Ceram Soc. 2019;102:3152–62.
33. Hirsch T, Lu Z, Stephan D. Impact of triethanolamine on the sulfate balance of Portland cements with mixed sulfate carriers. J Am Ceram Soc. 2021;104:4829–42.
34. European committee for standardization. EN 196-3:2017-03, Methods of testing cement - Part 3: Determination of setting times and soundness. Berlin: Beuth Verlag GmbH; 2017.
35. European committee for standardization. EN 196-1:2016-11, Methods of testing cement - Part 1: Determination of strength. Berlin: Beuth Verlag GmbH; 2016.
36. Jansen D, Stabler C, Goetz-Neunhoeffer F, Dittrich S, Neubauer J. Does ordinary Portland cement contain amorphous phase? A quantitative study using an external standard method. Powder Diffr. 2011;26:31–8.
37. Westphal T, Füllmann T, Pöllmann H. Rietveld quantification of amorphous portions with an internal standard—mathematical consequences of the experimental approach. Powder Diffr. 2009;24:239–43.
38. Nishi F, Takeuchi Y, Maki I. Tricalcium silicate $Ca_3O[SiO_4]$: the monoclinic superstructure. Z Kristallogr – Cryst Mater. 1985;172:297–314.
39. Mumme WG, Hill RJ, Bushnell-Wye G, Segnit ER. Rietveld crystal structure refinements, crystal chemistry and calculated powder diffraction data for the polymorphs of dicalcium silicate and related phases. Neues Jahrbuch für Mineralogie - Abhandlungen. 1995;169:35–68.
40. Mondal P, Jeffery JW. The crystal structure of tricalcium aluminate, $Ca_3Al_2O_6$. Acta Cryst B. 1975;31:689–97.
41. Nishi F, Takéuchi Y. The Al_6O_{18} rings of tetrahedra in the structure of $Ca_{8.5}NaAl_6O_{18}$. Acta Cryst B. 1975;31:1169–73.
42. Colville AA, Geller S. The crystal structure of brownmillerite, Ca_2FeAlO_5. Acta Cryst B. 1971;27:2311–5.
43. Sasaki S, Fujino K, Takeuchi Y. X-ray determination of electron-density distributions in oxides, MgO, MnO, CoO, and NiO, and atomic scattering factors of their constituent atoms. Proc Jpn Acad Ser B. 1979;55:43–8.
44. Markgraf SA, Reeder RJ. High-temperature structure refinements of calcite and magnesite. Am Mineral. 1985;70:590–600.
45. McGinnety JA. Redetermination of the structures of potassium sulphate and potassium chromate: the effect of electrostatic crystal forces upon observed bond lengths. Acta Cryst B. 1972;28:2845–52.
46. Henry PF, Weller MT, Wilson CC. Neutron powder diffraction in materials with incoherent scattering: an illustration of Rietveld refinement quality from nondeuterated gypsum. J Appl Crystallogr. 2009;42:1176–88.
47. Schmidt H, Paschke I, Freyer D, Voigt W. Water channel structure of bassanite at high air humidity: crystal structure of $CaSO_4{\cdot}0.625H_2O$. Acta Cryst B. 2011;67:467–75.
48. Cheng GCH, Zussman J. The crystal structure of anhydrite ($CaSO_4$). Acta Cryst. 1963;16:767–9.
49. Desgranges L, Grebille D, Calvarin G, Chevrier G, Floquet N, Niepce JC. Hydrogen thermal motion in calcium hydroxide: $Ca(OH)_2$. Acta Cryst B. 1993;49:812–7.
50. Goetz-Neunhoeffer F, Neubauer J. Refined ettringite ($Ca_6Al_2(SO_4)_3(OH)_{12}{\bullet}26H_2O$) structure for quantitative X-ray diffraction analysis. Powder Diffr. 2006;21:4–11.
51. Francois M, Renaudin G, Evrard O. A cementitious compound with composition $3CaO{\cdot}Al_2O_3{\cdot}CaCO_3{\cdot}11H_2O$. Acta Cryst. 1998;C59:1214–7.
52. Runčevski T, Dinnebier RE, Magdysyuk OV, Pöllmann H. Crystal structures of calcium hemicarboaluminate and carbonated calcium hemicarboaluminate from synchrotron powder diffraction data. Acta Cryst B. 2012;68:493–500.
53. Howard CJ, Sabine TM, Dickson F. Structural and thermal parameters for rutile and anatase. Acta Cryst B. 1991;47:462–8.
54. Wagner T, Kulik DA, Hingerl FF, Dmytrieva SV. GEM-selektor geochemical modeling package: TSolMod library and data interface for multicomponent phase models. Can Mineral. 2012;50:1173–95.
55. Kulik DA, Wagner T, Dmytrieva SV, Kosakowski G, Hingerl FF, Chudnenko KV, et al. GEM-Selektor geochemical modeling package: revised algorithm and GEMS3K numerical kernel for coupled simulation codes. Comput Geosci. 2013;26:189.
56. Thoenen T, Hummel W, Berner U, Curti E. The PSI/Nagra chemical thermodynamic data base 12/07. In: PSI Report 14-04, Villigen PSI, Switzerland. 2014. ISSN:1019-0643.
57. Lothenbach B, Zajac M. Application of thermodynamic modelling to hydrated cements. Cem Concr Res. 2019;123:105779.
58. European committee for standardization. EN 196-6:2018-12, Methods of testing cement - Part 6: Determination of fineness. Berlin: Beuth Verlag GmbH; 2018.
59. Ye S, Feng P, Liu Y, Liu J, Bullard JW. Dissolution and early hydration of tricalcium aluminate in aqueous sulfate solutions. Cem Concr Res. 2020;137:106191.
60. Lothenbach B, Winnefeld F. Thermodynamic modelling of the hydration of Portland cement. Cem Concr Res. 2006;36:209–26.
61. Lothenbach B, Le Saout G, Gallucci E, Scrivener KL. Influence of limestone on the hydration of Portland cements. Cem Concr Res. 2008;38:848–60.
62. Lothenbach B, Matschei T, Möschner G, Glasser FP. Thermodynamic modelling of the effect of temperature on the hydration

and porosity of Portland cement. Cem Concr Res. 2008;38:1–18.
63. Jansen D, Naber C, Ectors D, Lu Z, Kong X-M, Goetz-Neunhoeffer F, et al. The early hydration of OPC investigated by in-situ XRD, heat flow calorimetry, pore water analysis and ^{1}H NMR: learning about adsorbed ions from a complete mass balance approach. Cem Concr Res. 2018;109:230–42.
64. Jansen D, Goetz-Neunhoeffer F, Lothenbach B, Neubauer J. The early hydration of ordinary Portland cement (OPC): an approach comparing measured heat flow with calculated heat flow from QXRD. Cem Concr Res. 2012;42:134–8.
65. Lothenbach B, Kulik DA, Matschei T, Balonis M, Baquerizo L, et al. Cemdata18: a chemical thermodynamic database for hydrated Portland cements and alkali-activated materials. Cem Concr Res. 2019;115:472–506.
66. Dilnesa BZ, Wieland E, Lothenbach B, Dähn R, Scrivener KL. Fe-containing phases in hydrated cements. Cem Concr Res. 2014;58:45–55.
67. Matschei T, Lothenbach B, Glasser FP. The role of calcium carbonate in cement hydration. Cem Concr Res. 2007;37:551–8.
68. Bensted J. Thaumasite—direct, woodfordite and other possible formation routes. Cem Concr Compos. 2003;25:873–7.
69. Bensted J. Thaumasite—background and nature in deterioration of cements, mortars and concretes. Cem Concr Compos. 1999;21:117–21.
70. Schmidt T, Lothenbach B, Scrivener K, Romer M, Rentsch D, et al. Conditions of thaumasite formation. In: 12th international congress on the chemistry of cement (ICCC), Montreal, Canada, July 08–13, 2007; 2007.
71. Hartshorn SA, Sharp JH, Swamy RN. Thaumasite formation in Portland-limestone cement pastes. Cem Concr Res. 1999;29:1331–40.
72. Matschei T, Glasser FP. Thermal stability of thaumasite. Matér Constr. 2015;48:2277–89.
73. Jansen D, Goetz-Neunhoeffer F, Stabler C, Neubauer J. A remastered external standard method applied to the quantification of early OPC hydration. Cem Concr Res. 2011;41:602–8.
74. Begarin F, Garrault S, Nonat A, Nicoleau L. Hydration of alite containing aluminium. Adv Appl Ceram. 2011;110:127–30.
75. Pustovgar E, Mishra RK, Palacios M, d'Espinose de Lacaillerie J-B, Matschei T, et al. Influence of aluminates on the hydration kinetics of tricalcium silicate. Cem Concr Res. 2017;100:245–62.
76. Dorn T, Hirsch T, Stephan D. Influence of organic and inorganic accelerators on the Portland cement hydration and their applicability in 3D printing. In: European coating show 2019, Nürnberg, Germany, 18th–19th March 2019.
77. Aggoun S, Cheikh-Zouaoui M, Chikh N, Duval R. Effect of some admixtures on the setting time and strength evolution of cement pastes at early ages. Constr Build Mater. 2008;22:106–10.

SUPPORTING INFORMATION

Additional supporting information can be found online in the Supporting Information section at the end of this article.

How to cite this article: Dorn T, Hirsch T, Stephan D. Working mechanism of calcium nitrate as an accelerator for Portland cement hydration. J Am Ceram Soc. 2023;106:752–766. https://doi.org/10.1111/jace.18782